2014

Absorption Heat Transfer Performance of Ammonia-Water Mixture in 116 Tube Mini-Channel Heat Exchanger

Dennis Marijn van de Bor
TU Delft, Netherlands, The, d.m.vandebor@tudelft.nl

Carlos A. Infante Ferreira
TU Delft, Netherlands, The, C.A.InfanteFerreira@tudelft.nl

Absorption Heat Transfer Performance of Ammonia-Water Mixture in 116 Tubes Mini-Channel Heat Exchanger

Dennis Marijn VAN DE BOR[1]*, Carlos INFANTE FERREIRA[1]

[1]Delft University of Technology, Process & Energy Department,
Leeghwaterstraat 39, 2628 CB Delft, The Netherlands
+31152784894, d.m.vandebor@tudelft.nl

* Corresponding Author

ABSTRACT

It is known that decreasing the channel size in heat exchangers increases its heat and mass transfer performance. Using such heat exchangers offers the opportunity to reduce the size and cost of industrial heat pumps, what should lead to better market acceptance. In the past, many experiments have been done for air/water mixtures (adiabatic) and refrigerants like CO_2, R134a and water (diabatic). A variety of models predicting heat transfer coefficients for these refrigerants are available in literature, but for certain systems they are not in agreement with each other. Currently data for ammonia/water mixtures, a fluid used in absorption and compression-resorption heat pumps is missing.

A novel mini channel shell and tube heat exchanger with 116 tubes with an inner diameter of 0.5 mm, an outer diameter of 1.0 mm and a length of 0.655 m has been developed to increase the heat transfer performance in industrial compression-resorption heat pumps working with ammonia-water as refrigerant. In the current research the tube side heat transfer performance is investigated using the ammonia-water mixture, while water is used in the shell side of the heat exchanger. The influence of mass flow rate, heat load and vapor quality on the heat transfer performance and pressure drop are investigated.

The heat load was varied between 200 and 1800 W, with the refrigerant mass flux varied between 20 and 75 kg m^{-2} s^{-1} with the average vapor quality ranging between 0.2 and 0.6 kg kg^{-1} and operating pressures between 5 and 13 bar. Overall heat transfer coefficients, based on the outer diameter of the tubes, between 70 and 700 W m^{-2} s^{-1} have been obtained. The approach temperature at the absorber inlet, after calibrating the PT-100 elements, ranged between 0.3 and 4 K and the average temperature driving force is determined to be between 8 and 25 K. The measured pressure drop ranges between 0.02 and 0.2 bar. Trends show an increasing pressure drop and heat transfer coefficient with increasing mass flux and vapor quality. The heat transfer coefficient on the shell side appears to be the limiting factor at higher measured mass fluxes. The heat load was limited by the maximum flow of the water pumps on the shell side as well as the maximum available heating power of 3.5 kW.

1. INTRODUCTION

In order to reduce the amount of material used in a heat exchanger, and therefore possibly allowing for cost reduction of heat transfer equipment, brazed plate and mini-channel heat exchangers are investigated for pure fluids and mixtures. They are also of interest for sorption equipment (Cerezo et al., 2009, 2010, Taboas et al., 2010, 2012, van de Bor, 2014)

In this study the heat transfer performance of a novel mini-channel heat exchanger is investigated when an ammonia-water mixture flows through the tubes of a shell and tube heat exchanger at low flow rates. The results are compared with a slug flow model and empirical correlations for absorption in an annulus obtained from an earlier study (van de Bor, 2014).

2. EXPERIMENTAL SET-UP

A heat exchanger has been designed to be applied as the absorber of a compression resorption heat pump. It consists of 116 tubes with an internal diameter of 0.5 mm mounted within a shell with internal diameter of 21 mm. The heat exchanger has a vertical orientation and has a length of 0.655 m. The internal heat exchanging area is 0.119 m^2 while the external heat exchanging area is 0.239 m^2. Fractal distributors have been used to proportionally subdivide the main flow through the 116 tubes and guarantee pure countercurrent flow of tube and shell sides. Details of the fractal distributors and shell design can be viewed in Nefs et al. (2014).

Figure 1 shows the experimental set-up that has been used to determine the performance of the heat exchanger. It consists of two independent loops each used to create the required operating conditions in the tube side (left) and in the shell side (right) of the heat exchanger which is positioned centrally. Each loop includes a plate heat exchanger to create sub cooled conditions at the inlet of the circulating magnetically driven gear pumps. A coriolis flow meter allows for both measuring the flow and the density of the flow from which the ammonia-water concentration can be derived. A thermostatic bath brings the flow to the desired temperature level. To compensate for temperature losses before the inlet of the test section a thermostatically controlled tracing coil is used in the feed line. Since the experiments are intended to reproduce process operating conditions, the flows operate at temperature levels in the range 100 to 180°C.

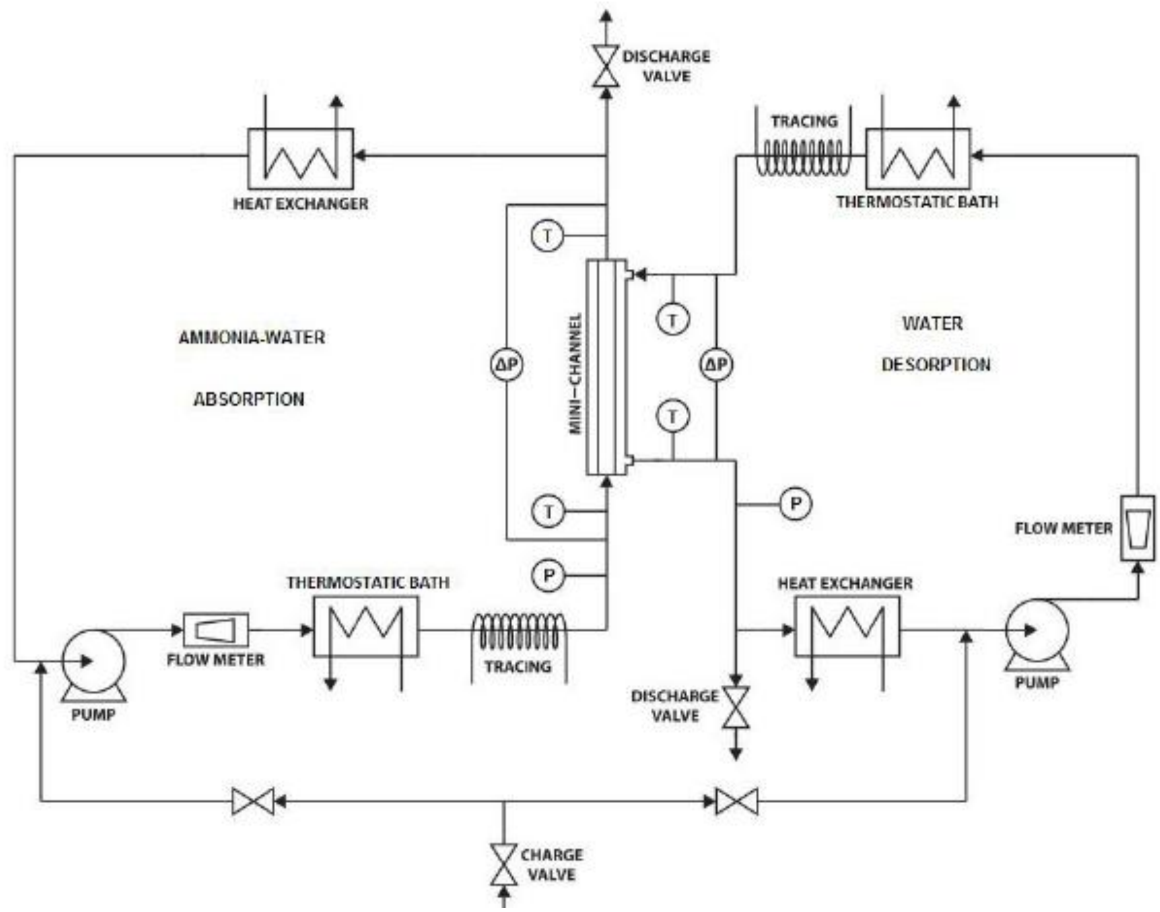

Figure 1: Schematic of the experimental set-up. The left side shows the ammonia-water absorption loop which corresponds to the tube side of the multi-tube mini-channel heat exchanger. The right side shows the cooling water loop which corresponds to the shell side of the heat exchanger.

In the here reported experiments absorption is taking place inside the tubes. The average ammonia concentration in the tube side loop is 35% (mass). In most of the here reported experiments water is heated up by the absorption process. In some experiments the water has been substituted by an ammonia-water flow with a slightly higher concentration. In these cases the ammonia-water desorption process taking place in the shell side represents the desorption of the process fluid.

Table 1: Geometrical data of the 116 tubes mini-channel heat exchanger

Position	**Values**	**Units**
Length heat exchanger	0.655	m
Number of tubes	116	
Inner diameter of tubes	0.5	mm
External diameter of tubes	1.0	mm
Inner diameter shell	21	mm
External diameter shell	25	mm
Hydraulic diameter shell side	1.8	mm

Table 1 summarizes the geometrical data of the heat exchanger. Figure 2 shows a cross section of the heat exchanger. The central area of the heat exchanger is filled with a massive rod which is used to fix the tube sheets. The tube arrangement is also visualized.

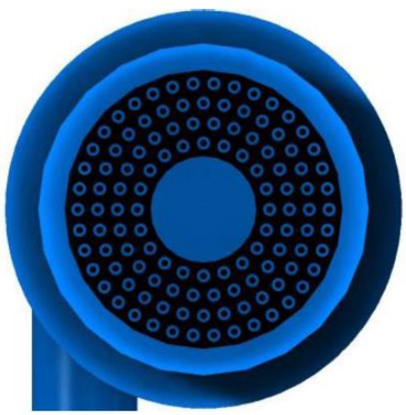

Figure 2: Cross section of the 116 tubes mini-channel heat exchanger. The internal diameter is 0.5 mm; the shell side hydraulic diameter is 1.8 mm.

During the experiments the average circulating concentration of ammonia in the solution was maintained constant at 35% mass. The inlet temperature has been maintained constant at both absorption and cooling water sides. The experimental conditions are summarized in Table 2. During the experiments the water was pressurized so that boiling could not occur in the shell side of the heat exchanger. The mass flow has been varied both on shell and tube sides. The absolute pressure was measured on both sides making use of Sitrans P DS III pressure sensors with an accuracy of 0.13 bar. The pressure drop was measured on both sides making use of Sitrans P DS III differential pressure sensors with an accuracy of 5.3 mbar. The in and outlet temperatures were measured with PT-100 sensors.

Table 2: Operating conditions

Experimental sets	**Tube side**	**Shell side**
Set 1: temperature [°C]	140	100
Set 2: temperature [°C]	160	100

3. EXPERIMENTAL RESULTS

3.1 Energy balance

The test section is insulated to prevent heat losses to the environment. Nevertheless it can be expected that the energy balance on the shell side gives a smaller heat load than the energy balance based on the tube side. The deviation between the heat loads calculated in both sides is an indication of the accuracy of the experiments. Figure 3 shows for 38 experiments how the two heat loads compare. As the figure shows some of the experiments have been discarded. These were the experiments for which the shell side balance indicated a higher heat load, what is not possible.

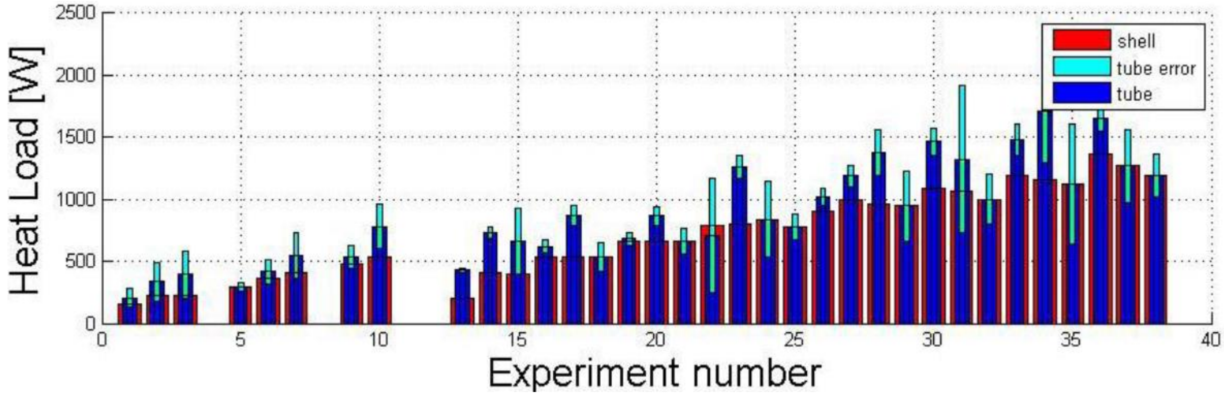

Figure 3: Comparison between the heat load based on tube side and shell sides. Experiments 4, 8, 11 and 12 showed difficulties with the data reduction and therefore are left out of the figure.

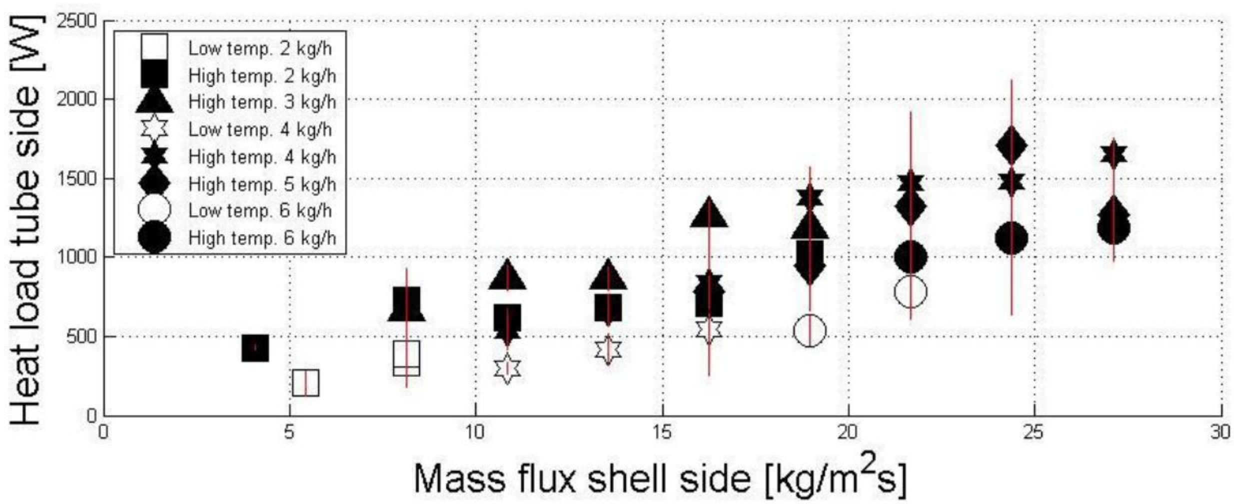

Figure 4: Tube side heat load as a function of shell side mass flux. The absorber (tube) side mass flow is also given. Since the operating conditions (inlet vapor fraction) varied during the experiments, a trend can not be recognized for the tube side.

Notice that, for the conditions of the experiments, the heat load varies from ca. 0.2 kW (1.7 kW/m^2) to 1.8 kW (15.1 kW/m^2). Higher heat loads were not feasible in the current set-up. Figure 4 shows the heat load as a function of the shell side mass flux with the mass flow in the tube side as a parameter. Due to small variations in temperature and pressure during the different tests it is possible that, against expectations, lower flow rates produces higher heat loads.

3.2 Pressure drop
Figure 5 shows the experimental pressure drop. It is clear that the pressure drop is quite low on both sides of the heat exchanger but that specifically in the shell side the pressure drop is extremely low.

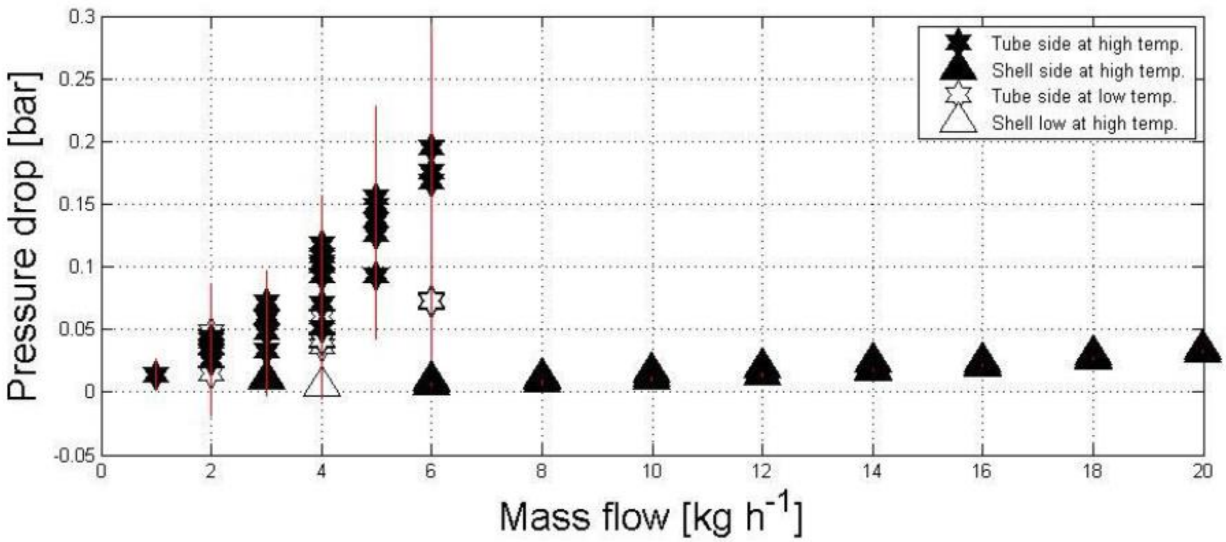

Figure 5: Experimental pressure in both tube side (mass flows have only been varied up to 6 kg/h due to limitations of the experimental set-up) in which absorption of ammonia in ammonia water solution is taking place and shell side in which water is flowing (mass flows are up to 20 kg/h).

3.3 Overall heat transfer coefficient
The overall heat transfer coefficient is derived from the experimental data making use of Equation (1).

$$U_S = \frac{\dot{Q}_{T,\exp}}{A_o \Delta T_{T,\exp}} \tag{1}$$

with

$$\dot{Q}_{T,\exp} = \dot{m}_{T,\exp}(h_{T,\exp,out} - h_{T,\exp,in}) \tag{2}$$

and

$$\Delta T_{T,\exp} = \sum_{i=1}^{n} \frac{(T_{T,i,in} - T_{S,i,out})(T_T, T_S, P_T, P_S)}{n} \tag{3}$$

Figure 6 shows the values of $\Delta T_{T,\exp}$ obtained for the different experiments. Finally the heat exchanging area is obtained from Equation (4). The resulting overall heat transfer coefficient is given in Figure 7.

$$A_o = \pi N_T d_{o,T} L_T \tag{4}$$

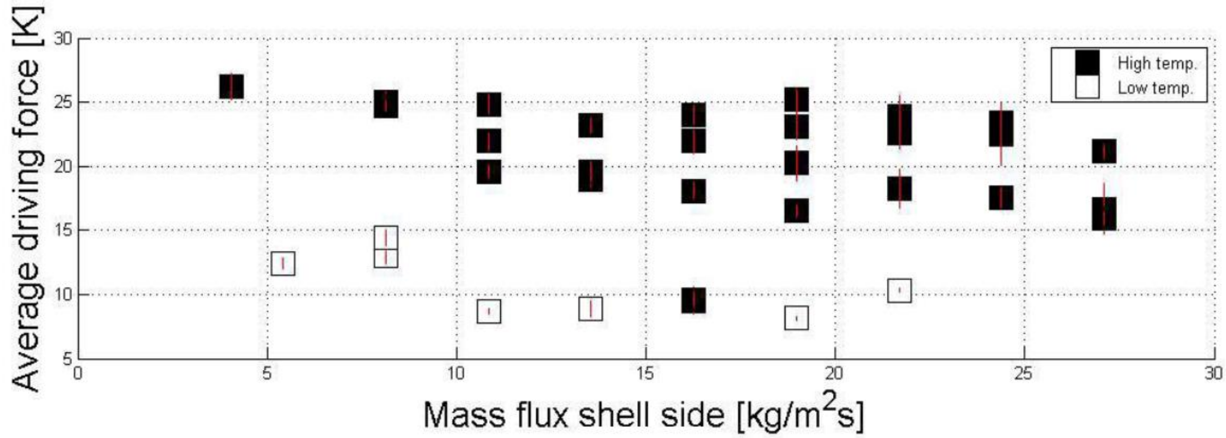

Figure 7: Temperature driving force for the different experiments shown as a function of the shell side mass flux.

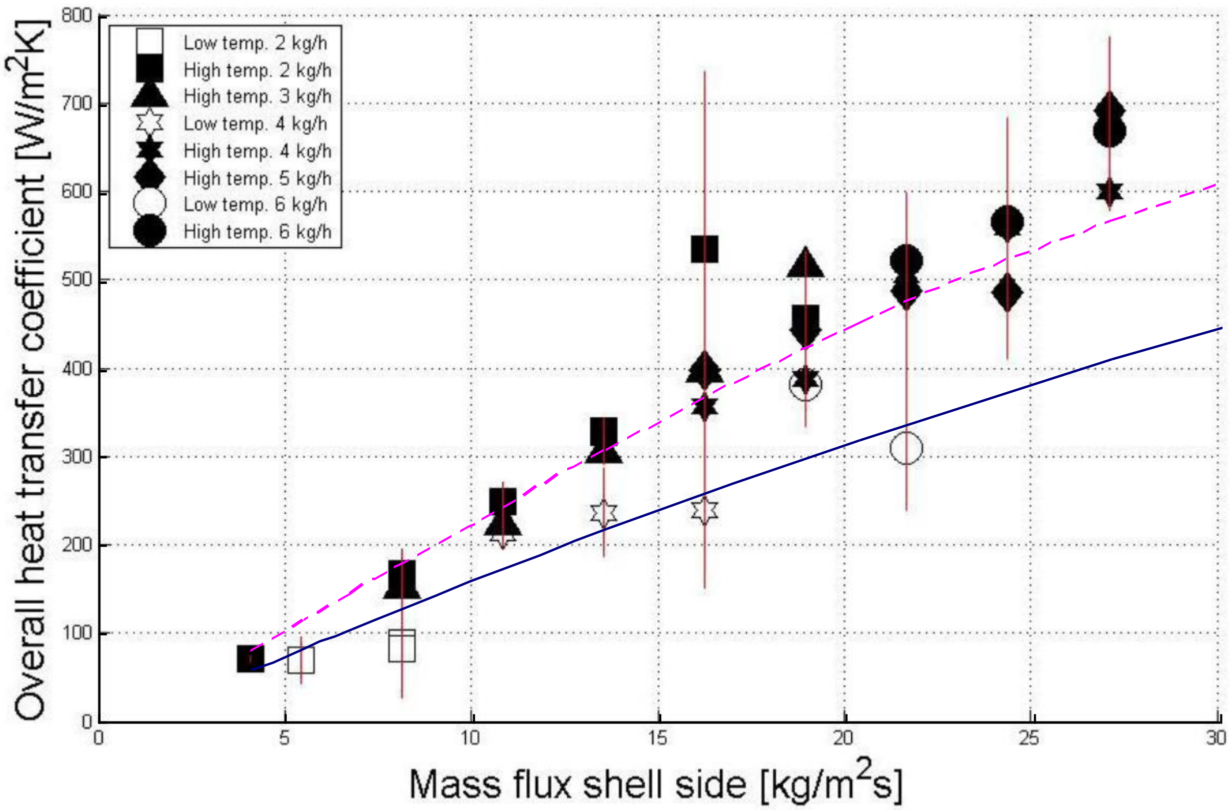

Figure 8: Overall heat transfer coefficient during the absorption experiments with ammonia-water in the tube side of the heat exchanger and water in the shell side. The lines represent the equation proposed by van de Bor (2014) for the average heat flux across the heat exchanger surface.

Although both shell and tube side mass fluxes are quite small, the overall heat transfer coefficient can reach up to 0.7 kW m^{-2} K^{-1} as presented in Figure 8. Again, small variations in temperature and pressure during the different tests it is possible that, against expectations, lower flow rates produces higher heat loads. This in turn has its effect on the heat transfer coefficient presented in Figure 8.

4. DISCUSSION

4.1 Expected temperature profiles

Considering the heat transfer performance of single tube experiments (van de Bor, 2014) it can be expected that significantly higher performance should be attained. A model of the processes in the heat exchanger assuming an annular flow in the tubes indicates however that the temperature differences along the heat exchanger length are not constant for the operating conditions of the heat exchanger. This is illustrated in Figure 9 where the temperature profiles in the heat exchanger are indicated.

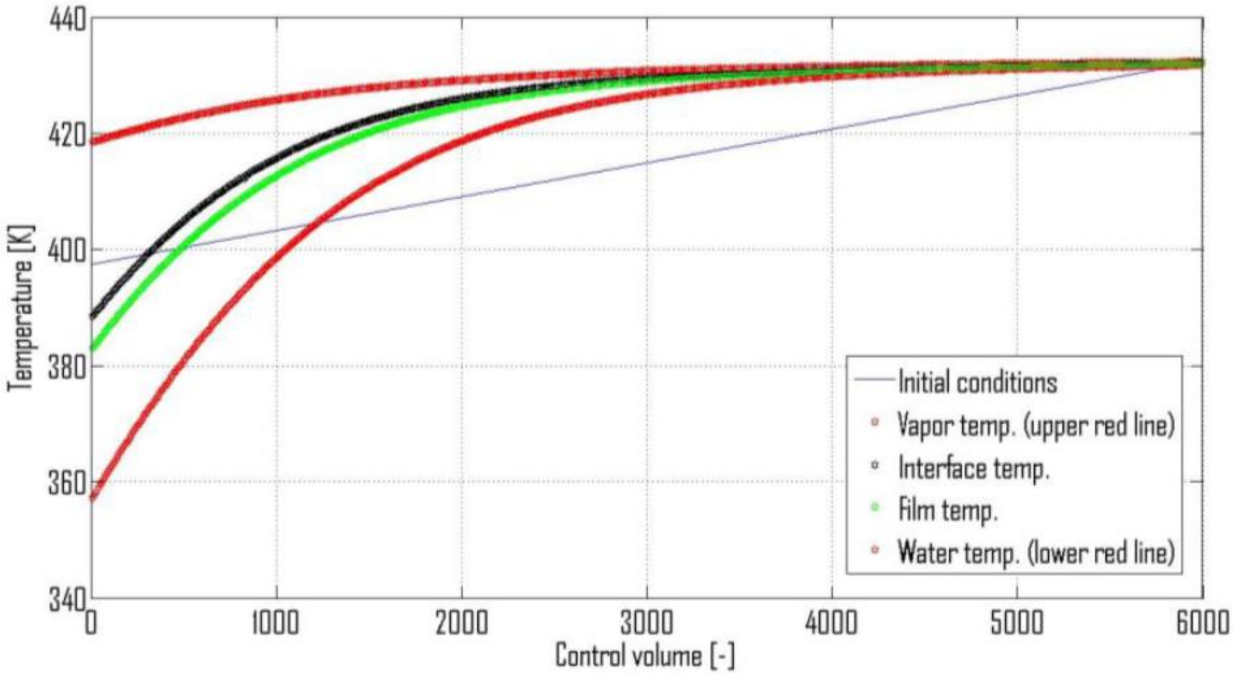

Figure 9: Numerically predicted temperature profiles along the heat exchanger length. The water flow appears to heat up very quickly so that the temperature driving force becomes very small for 50% of the heat exchanger area. The model assumes annular flow so that heat transfer takes place from liquid film to water.

In the present simulation the water flow enters with 84°C and leaves with 159.9°C. With a shell side flow of 10.1 kg/m^2s, the mass flow is 2.78 g/s so that 898 W are exchanged. In the tube side ammonia is being absorbed. The flow is 4 kg/h so that, at 15 bar operating pressure, the temperature would drop from 160°C to 124°C when liquid and vapor would be in equilibrium. The model expects the liquid film to cool down to 110°C while the vapor phase remains at 147°C. At the outlet there is still 12.5% vapor left, explaining why the assumption of equilibrium leads to higher temperatures. In reality the temperature driving force is close to 0 for about 50% of the area of the heat exchanger. The assumption of equilibrium in the absorption side leads to an average temperature driving force of 24.6 K. The model indicates an average temperature driving force between liquid film and water flow of 9.1 K. This indicates that the overall heat transfer coefficient is 2.7 times larger than indicated in Figure 7.

4.2 Expected temperature profiles

In van de Bor (2014) an empirical correlation was proposed for the absorption side heat transfer coefficient in mini-channel annuli. Adjusting this equation for absorption inside tubes by changing the surface area to the inner tube area results in equation 5. The shell-side heat transfer coefficient has been obtained from Nefs et al. (2014).

$$\alpha_{abs} = 0.0079\left(\frac{\dot{Q}}{A_i}\right)^{1.29} \tag{5}$$

Although the empirical correlations proposed by van de Bor (2014) were derived to obtain the absorption side heat transfer coefficient in an annulus at higher velocities, the function derived at low absorption side inlet temperatures (and consequently low heat loads) is capable of predicting the heat transfer coefficient of most of the experiments within the margin of error of the experiments. This is illustrated in Figure 7 in which the correlation derived by van de Bor (2014) has been applied for the tube side experiments.

From van de Bor (2014) it appears that significantly higher absorption heat transfer coefficients can also be attained for heat flux above 50 kW m^{-2} K^{-1} while in these experiments the heat flux remains below 15 kW m^{-2} K^{-1}

4.3 Pressure drop

The results for the pressure drop have been compared with the gas-liquid pressure drop equation proposed by Zhang et al. (2010). This model over predicts the tube side pressure drop at low measured values, the prediction is better at higher pressure drop values. Similar results were obtained in van de Bor (2014), see Fig. 10.

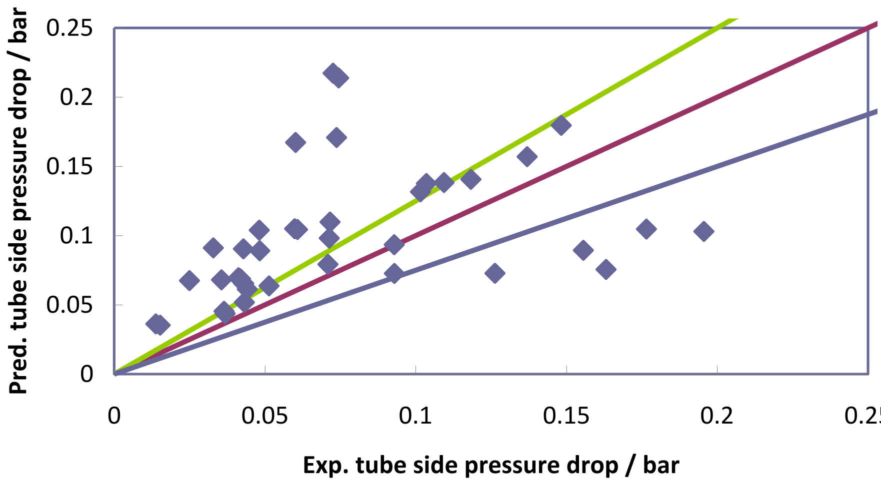

Figure 10: The pressure drop model by Zhang et al. (2010) tends to slightly overpredict the tube side pressure drop. The lines indicate the +25%/0/-25% error band

6. CONCLUSIONS

- The heat transfer coefficient increases with increasing heat load
- Tested flow rates are too low to obtain maximum heat transfer performance
- Pressure drop increases with increasing flow rate and vapor quality
- The annular flow model predicts larger heat transfer coefficients than obtained from the measurements assuming equilibrium conditions and constant heat flux along the tube
- Annular flow might not occur at low flow rates, additional resistances might exist that were not modeled or the heat exchanger loading is too low.

NOMENCLATURE

A	area	(m^2)

d	diameter	(m)
h	enthalpy	(J kg^{-1})
L	length	(m)
$\dot{m}$	mass flux	(kg s^{-1})
n	number of control volumes	(-)
N	number of tubes	(-)
P	pressure	(Pa)
$\dot{Q}$	heat load	(W)
T	temperature	(C)
U	overall heat transfer coefficient	(W m^{-2} K^{-1})
α	Heat transfer coefficient	(W m^{-2} K^{-1})

Subscript

Abs	absorption
exp	experimental
i	inside
in	inlet
o	outside
out	outlet
S	shell side
T	tube side, total

REFERENCES

Van de Bor, D.M., 2014, Mini-channel heat exchangers for industrial distillation processes. *PhD thesis*. Delft University of Technology, Delft, the Netherlands.

Cerezo, J., Bourouis M., Vallès M., Coronas A., Best R., 2009, Experimental study of an ammonia–water bubble absorber using a plate heat exchanger for absorption refrigeration machines, *Appl Therm Eng.*, vol 29, p. 1005-1011.

Cerezo, J., Best R., Bourouis M., Coronas, A., 2010, Comparison of numerical and experimental performance criteria of an ammonia–water bubble absorber using plate heat exchangers, *Int. J. Heat Mass Trans*., vol 53, no. 17-18: p. 3379–3386.

Nefs, C.W.M., Van de Bor, D.M., Infante Ferreira, C.A., 2014, Laminar single phase flow distribution in a multi-tube mini-channel exchanger using fractal distribution, *Chem. Eng. Process.*, available online april 8, 2014

Táboas, F., Vallès, M., Bourouis M., Coronas, A., 2010, Flow boiling heat transfer of ammonia/water mixture in a plate heat exchanger, *Int. J. Refrig*., vol. 33, no. 4: p. 695-705.

Táboas, F., Vallès, M., Bourouis M., Coronas, A., 2012, Assessment of boiling heat transfer and pressure drop correlations of ammonia/water mixture in a plate heat exchanger, *Int. J. Refrig*., vol. 35, no. 3: p. 633-644.

Zhang, W., Hibiki, T., Mishima, K., 2010, Correlations of two-phase frictional pressure drop and void fraction in mini-channel, *Int. J. Heat Mass Trans*., vol. 53, no. 1-3: p. 453–465.

ACKNOWLEDGEMENT

The authors want to acknowledge Florijn de Graaf, Hilde Koopmans, Pascal Smulders and Stijn ten Pas for their efforts in collecting the experimental data reported in this paper.

This is an ISPT (=Institute for Sustainable Process Technology) project.